

Non-standing spin-waves in confined micrometer-sized ferromagnetic structures under uniform excitation

Cite as: Appl. Phys. Lett. **116**, 072401 (2020); <https://doi.org/10.1063/1.5139881>

Submitted: 22 November 2019 . Accepted: 26 January 2020 . Published Online: 18 February 2020

S. Pile , T. Feggeler , T. Schaffers , R. Meckenstock, M. Buchner, D. Spoddig , B. Zingsem , V. Ney , M. Farle , H. Wende , H. Ohldag , A. Ney , and K. Ollefs 

COLLECTIONS

 This paper was selected as an Editor's Pick



View Online



Export Citation



CrossMark

ARTICLES YOU MAY BE INTERESTED IN

[Ti- and Fe-related charge transition levels in \$\beta\$ -Ga₂O₃](#)

Applied Physics Letters **116**, 072101 (2020); <https://doi.org/10.1063/1.5139402>

[Development of a silicon-diamond interface on \(111\) diamond](#)

Applied Physics Letters **116**, 071602 (2020); <https://doi.org/10.1063/1.5144093>

[Reduced spin torque nano-oscillator linewidth using He⁺ irradiation](#)

Applied Physics Letters **116**, 072403 (2020); <https://doi.org/10.1063/1.5137837>

Lock-in Amplifiers
up to 600 MHz



Non-standing spin-waves in confined micrometer-sized ferromagnetic structures under uniform excitation

Cite as: Appl. Phys. Lett. **116**, 072401 (2020); doi: 10.1063/1.5139881

Submitted: 22 November 2019 · Accepted: 26 January 2020 ·

Published Online: 18 February 2020



View Online



Export Citation



CrossMark

S. Pile,^{1,a)}  T. Feggeler,²  T. Schaffers,^{1,b)}  R. Meckenstock,² M. Buchner,¹ D. Spoddig,²  B. Zingsem,^{2,3} 
V. Ney,¹  M. Farle,^{2,4}  H. Wende,²  H. Ohldag,^{5,6,c)}  A. Ney,¹  and K. Ollefs² 

AFFILIATIONS

¹Institute of Semiconductor and Solid State Physics, Johannes Kepler University Linz, 4040 Linz, Austria

²Faculty of Physics and Center for Nanointegration Duisburg-Essen (CENIDE), University of Duisburg-Essen, 47057 Duisburg, Germany

³Ernst Ruska-Centrum für Mikroskopie und Spektroskopie mit Elektronen, Forschungszentrum Julich GmbH, D-52425 Julich, Germany

⁴Kirensky Institute of Physics, Federal Research Center KSC SB RAS, Krasnoyarsk 660036, Russia

⁵Stanford Synchrotron Radiation Laboratory, SLAC National Accelerator Laboratory, Menlo Park, California 94025, USA

⁶Department of Physics, University of California Santa Cruz, Santa Cruz, California 95064, USA

^{a)}Author to whom correspondence should be addressed: santa.pile@jku.at

^{b)}Present address: NanoSpin, Department of Applied Physics, Aalto University School of Science, P.O. Box 15100, FI-00076 Aalto, Finland.

^{c)}Present addresses: Advanced Light Source, Lawrence Berkeley National Laboratory, Berkeley, CA 94720, USA and Department of Material Sciences and Engineering, Stanford University, Stanford, CA 94305, USA.

ABSTRACT

A non-standing characteristic of directly imaged spin-waves in confined micrometer-sized ultrathin Permalloy ($\text{Ni}_{80}\text{Fe}_{20}$) structures is reported along with evidence of the possibility to alter the observed state by modifications to the sample geometry. Using micromagnetic simulations, the presence of the spin-wave modes excited in the Permalloy stripes along with the quasi-uniform modes was observed. The predicted spin-waves were imaged in direct space using time resolved scanning transmission x-ray microscopy, combined with a ferromagnetic resonance excitation scheme (STXM-FMR). STXM-FMR measurements revealed a non-standing characteristic of the spin-waves. Also, it was shown by micromagnetic simulations and confirmed using STXM-FMR results that the observed characteristic of the spin-waves can be influenced by the local magnetic fields in different sample geometries.

© 2020 Author(s). All article content, except where otherwise noted, is licensed under a Creative Commons Attribution (CC BY) license (<http://creativecommons.org/licenses/by/4.0/>). <https://doi.org/10.1063/1.5139881>

The substitution of electrons by photons or quasi-particles such as magnons is of great importance for potential alternative developments in future computing technologies.¹ This technology will move much closer toward real applications, if one is able to actually make use of these quasi-particles. Prerequisites for that are well-investigated and understood properties of the particles and thus the possibility to control their behavior.^{2–4} The scope of our research is the investigation of magnetization dynamics as it provides an opportunity for highly advanced magnetic memory and logic devices.^{5–7}

Magnons or spin-waves, being the elementary excitations of coupled spin systems in solids, have been widely investigated in thin

films,^{8–10} nanostructured multilayers,¹¹ magnonic crystals,^{12–15} and magnonic waveguides.^{16–18} Spin-waves in confined micrometer-sized structures have also drawn increasing interest^{19,20} as understanding of their dynamics is of utmost importance for the development of computational devices, the size of which is decreasing over the time.

The experimental investigation on such a small scale requires very sensitive experimental techniques. Moreover, if one wants to obtain information about time and space resolved magnetization dynamics, the measuring techniques are required to be quite sophisticated. The possibility to excite and visualize spin-waves in micrometer-sized structures was shown to be possible by techniques

such as Brillouin light scattering (BLS)^{20,21} or spatially resolved ferromagnetic resonance force microscopy (FMRFM).²² Later time-resolved scanning transmission x-ray microscopy (TR-STXM)^{23–25} has been combined with a phase-locked ferromagnetic resonance (FMR) excitation scheme (STXM-FMR). This recently reported STXM-FMR technique enables direct time-dependent imaging of the spatial distribution of the precessing magnetization over the sample during FMR excitation.^{26–29}

In most of the cases, spin-waves are investigated using a non-uniform excitation of the structure.^{2,4,10,12} When the uniform excitation field is applied to the specimen, it is also possible to excite spin-waves, but only standing spin-waves are expected.³⁰ A standing spin-wave implies that its nodes remain at the same position in space over the time. In case when the out-of-plane component of the in-plane precessing magnetization forms the wave, the nodes are the regions with zero out-of-plane magnetization. The development of planar micro-resonators allowed us to measure the spin-wave spectrum of a single micrometer-sized stripe using the conventional FMR technique.^{31–34} Using this technique, the presence of spin-waves in a single micrometer-sized Permalloy stripe during its uniform excitation was evidenced earlier with the support of micromagnetic simulations.³³ To be detectable by FMR, the spin-waves in the micrometer-sized stripe need to exhibit a standing characteristic and thus provide a net absorption signal under excitation with a homogeneous microwave field. These findings were corroborated by detailed investigations of comparable spin-wave modes in a Co micrometer-sized stripe with similar dimensions.³⁴

To be able to directly image spin-wave modes reported previously,^{33,34} we used a model system of two identical micrometer-sized Permalloy stripes to investigate different orientations of the stripe relative to the external magnetic field under the same conditions. Each of the stripes has a lateral dimension of $1 \times 5 \mu\text{m}^2$ and a thickness of 30 nm with 5 nm Al capping to protect Permalloy against oxidation. The stripes were oriented perpendicular to each other with a gap of $2 \mu\text{m}$ between them. In the chosen experimental geometry, the external static magnetic field B_{ext} was oriented in-plane along the length of one stripe (“easy orientation”) and perpendicular to the length of the other (“hard orientation”).³⁴ Two sample systems were taken into consideration: the so-called “T-geometry” with the stripe in easy orientation centered to the middle of the length of the stripe in hard orientation [see Figs. 2(b) and 3(a)] and “L-geometry” with the stripe in easy orientation aligned to one of the shorter edges of the stripe in hard orientation [see Fig. 3(c)].

To determine B_{ext} at which the quasi-uniform and spin-wave modes occur with the FMR excitation scheme at the microwave frequency of $f_{\text{MW}} = 9.446 \text{ GHz}$, MuMax3³⁵ micromagnetic simulations were performed to calculate the FMR spectrum for both geometries of the samples. In Figs. 1(a) and 1(b), simulated FMR spectra of the T- and L-geometries are shown, respectively. Additionally, the spatial distribution of the magnetic excitations was calculated at each simulated point of the spectra. The direction of the external field relative to the samples’ orientation is shown in the insets corresponding to signals no. 1 and 5 in the figure. Comparison of the simulated FMR spectra of both sample systems shows the same resonance field positions [see Figs. 1(a) and 1(b)]. Simulated spatial distributions of the magnetic excitations are displayed in the insets of Fig. 1 for signals 1–4 and 5–8, respectively. Red and blue colors in the images indicate the opposite

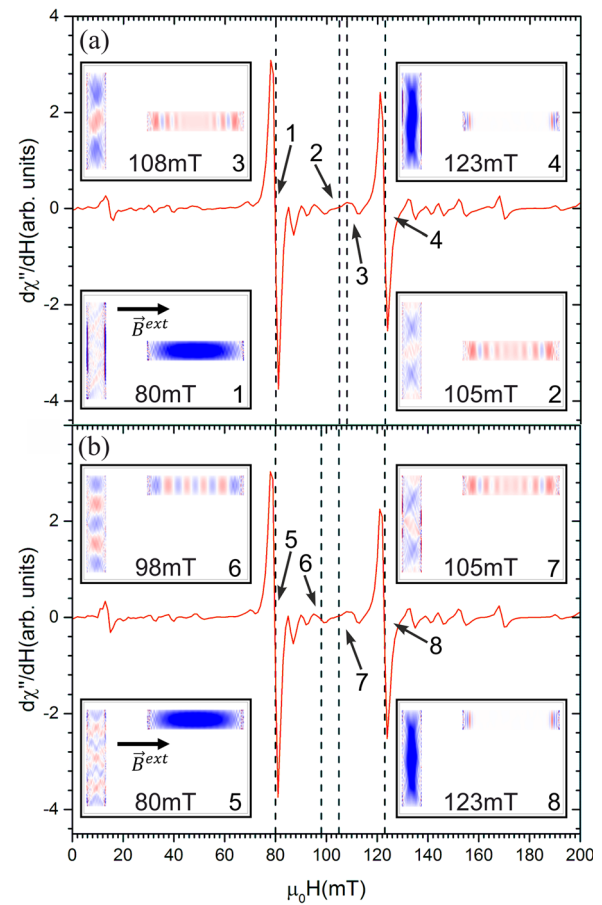


FIG. 1. MuMax3 simulations of the FMR spectrum and the spatial distribution of the out-of-plane component of the magnetization in the Permalloy micrometer-sized stripes in (a) T-geometry and (b) L-geometry.

orientation of the dynamic out-of-plane component of the magnetisation, and the value of the component is indicated by the color intensity. The white color in the simulation images represents zero out-of-plane magnetization component. The spatial distribution in Fig. 1 is represented for several external magnetic field values. The results of the simulations show that the largest FMR signals at 80 mT (signal nos. 1 and 5) and 123 mT (signal nos. 4 and 8) are quasi-uniform modes of the stripes in easy and hard orientation, respectively. The separation in the field values for the quasi-uniform modes of two perpendicular stripes of one sample is a result of shape anisotropy. The smaller signals observed in the spectra are the spin-wave modes of the two stripes.^{33,34}

Although there was no difference in the FMR spectra, the spatial distribution of the magnetic excitations shows a distinct difference between T- and L-geometries at certain external field values. One of the examples is shown in the insets corresponding to signal nos. 2 and 7 in Fig. 1 for the external field of 105 mT. The spatial distribution of the magnetic excitations in the stripe in hard orientation shows asymmetry of the nodes along the length of the stripe in the L-geometry in comparison to the T-geometry, where the

nodes are situated symmetrically along the stripe length with respect to the stripe center.

FMR is excited by applying a small periodic magnetic field perpendicular to the direction of the static field B_{ext} , which is applied in the film plane.^{31–34} When the FMR condition is fulfilled, a persistent precession of the magnetization around the direction of the effective magnetic field occurs. In the case of in-plane magnetization [see Fig. 2(b)], the dynamic component of the precessing magnetization perpendicular to the sample surface can be probed in the STXM-FMR by circularly polarized x-ray photons at the $L_{2/3}$ -edges of a

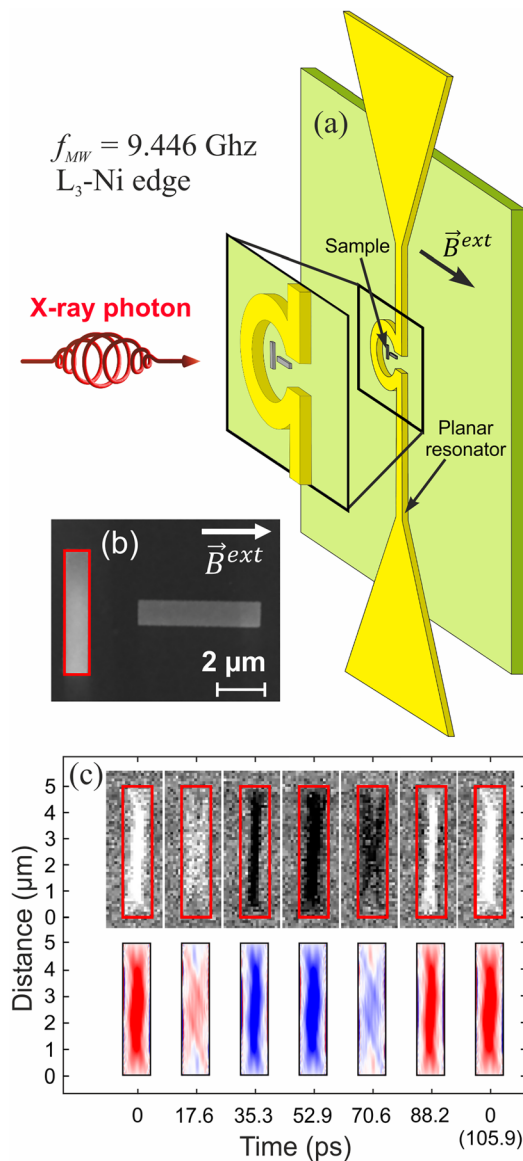


FIG. 2. (a) Sketch of the STXM-FMR experiment geometry, (b) scanning electron microscope image of the sample in T-geometry, and (c) results of the STXM-FMR measurements at 123 mT for the stripe in hard orientation in the T-geometry sample and corresponding micromagnetic simulations.

ferromagnet passing through the sample perpendicular to its plane as shown schematically in Fig. 2(a).^{26,27} The transmitted light intensity depends on the relative directions of the x-rays' polarization and dynamic component of the magnetization, the so-called x-ray magnetic circular dichroism (XMCD) effect. Thus, the maximum and minimum intensities on the STXM-FMR images (white and black contrast in the scans) mean the maximum deviation of the dynamic component of the magnetisation in opposite directions.²⁹

The STXM-FMR measurements were carried out at a Ni L_3 -edge at the microwave excitation frequency of $f_{MW} = 9.446$ GHz. An example of the STXM-FMR measurement of the stripe in hard orientation [marked with the red rectangle in Fig. 2(b)] in T-geometry is demonstrated in the upper row of the images (STXM-FMR scans) in Fig. 2(c). The scans represent six equidistant time-steps of the magnetisation precession cycle depicting the dynamics of the quasi-uniform mode at 123 mT. The seventh point in time is always included, which is a repetition of the results of the first one to demonstrate the full period of the recorded signal. The stripe area is marked with a red rectangle. Below each STXM image in Fig. 2(c), a snapshot of the corresponding micromagnetic simulation is shown, i.e., excitation no. 4 in Fig. 1(a). One can directly observe that in the quasi-uniform mode, the magnetic moments of the sample precess in phase across almost its entire area. This can be seen from the STXM-FMR images where the magnetic contrast across the sample area changes its color from white [0 ps in Fig. 2(c)] to black [52.9 ps in Fig. 2(c)] after a half of the precession period of 105.9 ps, while the background contrast remains the same. The non-uniformity of the precession closer to the stripe edges stems from a non-uniform effective field inside the sample, originating from the strong demagnetising fields closer to the stripe's edges.¹⁹ The overall agreement between the dynamic magnetic contrast of the STXM-FMR measurement and the micromagnetic simulation is remarkable and can be taken as experimental proof of the validity and credibility of the simulations.

The STXM-FMR results at the Ni L_3 -edge for the spin-wave mode of the sample in T-geometry at 108 mT are shown in Fig. 3(b). One can clearly distinguish three regions within the stripe (inside the red rectangle) with opposite orientation of the dynamic magnetization component. This indicates the presence of a spin-wave mode at the given external field. The red dots on the scans are used to indicate the position of the nodes of the observed spin-wave. It is visible in the plot that the nodes do not remain at the same position within the stripe over time, which demonstrates that no purely standing spin-wave is observed. The same behavior can be seen in the simulated spatial distribution plotted in Fig. 3(b) following the white spaces between red and blue regions in the stripe. An external field of 108 mT corresponds to signal no. 3 in Fig. 1(a). This is not a resonance field of a spin-wave mode within the sample, but 3 mT below the closest one at 111 mT. Hence, spin excitation observed in the STXM-FMR measurement is not a single eigenmode.²⁰ Instead, inhomogeneities produced by internal magnetization landscapes of the stripe and inhomogeneous external magnetic stray fields, caused by the second stripe, can lead to a superposition of spin-wave eigenmodes, resulting in the observed movement of the nodes. The observed movement is an evidence of the possibility to excite non-standing spin-waves in confined structures using uniform excitation by a microwave field.

The STXM-FMR measurements of the L-geometry sample were carried out under identical experimental conditions as for the

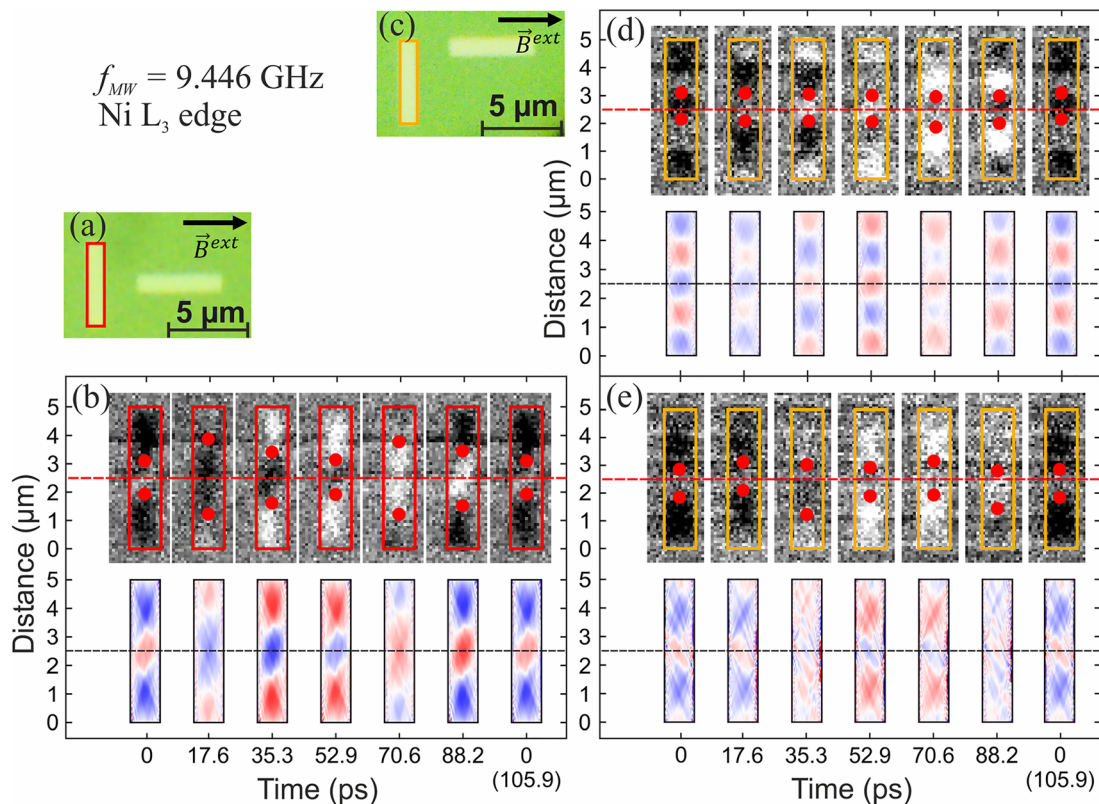


FIG. 3. (a) Optical image of the sample in T-geometry and its (b) results of the STXM-FMR measurements at 108 mT for the stripe in hard orientation and corresponding micromagnetic simulations. (c) Optical image of the sample in L-geometry and its (d) results of the STXM-FMR measurements at 98 mT and (e) 105 mT for the stripe in hard orientation and corresponding micromagnetic simulations.

T-geometry. The results of two of these measurements are shown in Figs. 3(d) and 3(e) at fields of 98 mT and 105 mT, respectively. The stripe area is marked with orange rectangles in the STXM-FMR images. The dynamic magnetic contrast at 98 mT [see Fig. 3(d)] is very close to a standing mode as the position of the nodes marked with red dots does not change significantly along the stripe over the time. This observation is confirmed by simulations plotted below the STXM-FMR scans in Fig. 3(d). Also, the FMR simulation in Fig. 1(b) shows that signal no. 6 is only 1 mT off from the resonance field of the spin-wave mode at 97 mT.

In contrast, the results at 105 mT exhibit a non-standing characteristic of the observed spin-wave, which can be concluded from the change in the position of the nodes in Fig. 3(e). Notably, the observed movement of the nodes at this field in L-geometry is asymmetric relative to the center of the stripe marked with the red dashed horizontal line in Fig. 3(e). This can be seen, for example, when comparing scans at 0 ps and 17.6 ps points in time in Fig. 3(e): from the first scan to the second, both nodes are shifted slightly upwards. The field of 105 mT corresponds to signal no. 7 in Fig. 1(b), which is 6 mT below the closest resonance field of the spin-wave mode. As discussed before, a superposition of the spin-wave eigenmodes takes place in combination with the inhomogeneity of the external stray fields being shifted with the second stripe to the upper shorter edge of the stripe in question. Therefore, the asymmetric behavior of the spin-wave dynamics can be

linked to the inhomogeneity of the external field, which in the case of the L-geometry is asymmetric.

Directly observed spin-waves are the result of the interference of the waves in several directions.^{2,8,36} It was reported earlier that edge roughness of the sample, edge surface profile,¹⁸ its shape,² or micro variations of the external field applied during excitation³⁷ can cause significant changes in the spin-wave dispersion in one or several directions, leading to different behavior of the resulting excitation pattern. In the case of mode no. 6 in Fig. 3(f), we still observe a slight variation of the nodes' position in space, which can be a result of not perfectly hitting the resonance field value and/or a roughness of the sample edges. It is possible that with a very small shift of the resonance field, the standing characteristic of the wave changes to the non-standing one when the transition and/or superposition between the eigenmodes occurs. This kind of movement is not possible to detect using the conventional FMR technique, but it is possible to image it directly using STXM-FMR. The additional influence of the second stripe can lead to local disturbances, affecting the spin-wave dispersion in one or several directions, and hence, this leads to an observable asymmetry of the nodes' movement of the resulting wave.

In conclusion, our STXM-FMR experiments have shown that it is possible to directly observe quasi-uniform and spin-wave modes that can be detected using the FMR technique in micrometer-sized Permalloy stripes, as well as dynamic magnetic excitations between the

FMR-lines. More importantly, in-between, we demonstrated the possibility to slightly alter the spin-wave behavior in the stripe in the hard orientation, by placing the second stripe (easy orientation) at different positions along its length. The sample geometry allows us to modify the magnetic field inhomogeneity within one of the stripes, thus leading to the change in the spin-wave behavior. This concept has great potential as Permalloy is a very widely used material and a shape modification is much more easily achievable than the modification of the crystalline structure required for a number of materials used for inducing propagating spin-waves.

The use of the Stanford Synchrotron Radiation Lightsource, SLAC National Accelerator Laboratory, is supported by the U.S. Department of Energy, Office of Science, Office of Basic Energy Sciences under Contract No. DE-AC02-76SF00515. The authors would like to thank the Austrian Science Foundation (FWF), Project No. I-3050 as well as the German Research Foundation (DFG), Project No. OL513/1-1 for financial support. K.O., H.W., B.Z and M.F. acknowledge additional funding from Deutsche Forschungsgemeinschaft (DFG, German Research Foundation) – Project-ID 405553726 – TRR 270 and B.Z and M.F. acknowledge additional funding from Research Grant No. 075-15-2019-1886 from the Government of the Russian Federation.

REFERENCES

- ¹A. Chumak, V. Vasyuchka, A. Serga, and B. Hillebrands, *Nat. Phys.* **11**, 453–461 (2015).
- ²P. Clausen, K. Vogt, H. Schultheiss, S. Schäfer, B. Obry, G. Wolf, P. Pirro, B. Leven, and B. Hillebrands, *Appl. Phys. Lett.* **99**, 162505 (2011).
- ³D. Grundler, *Nat. Phys.* **11**, 438–441 (2015).
- ⁴M. Vogel, R. Aßmann, P. Pirro, A. V. Chumak, B. Hillebrands, and G. Freymann, *Sci. Rep.* **8**, 11099 (2018).
- ⁵Q. Wang, P. Pirro, R. Verba, A. Slavin, B. Hillebrands, and A. Chumak, *Sci. Adv.* **4**(1), e1701517 (2018).
- ⁶T. Brächer, P. Pirro, and B. Hillebrands, *Phys. Rep.* **699**, 1–34 (2017).
- ⁷V. Vlaminck and M. Bailleul, *Science* **322**, 410 (2008).
- ⁸B. Kalinikos and A. Slavin, *J. Phys. C*: **19**, 7013–7033 (1986).
- ⁹H. Yu, R. Huber, T. Schwarze, F. Brand, T. Rapp, P. Berberich, G. Duerr, and D. Grundler, *Appl. Phys. Lett.* **100**, 262412 (2012).
- ¹⁰O. Gladii, M. Haidar, Y. Henry, M. Kostylev, and M. Bailleul, *Phys. Rev. B* **93**, 054430 (2016).
- ¹¹M. Madami, S. Bonetti, G. Consolo, S. Tacchi, G. Carlotti, G. Gubbiotti, F. B. Mancoff, and J. Å. M. A. Yar, *Nat. Nanotechnol.* **6**, 635–638 (2011).
- ¹²A. V. Chumak, P. Pirro, A. A. Serga, M. P. Kostylev, R. L. Stamps, H. Schultheiss, K. Vogt, S. J. Hermsdoerfer, B. Laegel, P. A. Beck, and B. Hillebrands, *Appl. Phys. Lett.* **95**, 262508 (2009).
- ¹³S. Neusser, G. Duerr, S. Tacchi, M. Madami, M. L. Sokolovskyy, G. Gubbiotti, M. Krawczyk, and D. Grundler, *Phys. Rev. B* **84**, 094454 (2011).
- ¹⁴J. Gräfe, M. Weigand, C. Stahl, N. Träger, M. Kopp, G. Schütz, and E. J. Goering, *Phys. Rev. B* **93**, 014406 (2016).
- ¹⁵M. Langer, R. Gallardo, T. Schneider, S. Stienen, A. Roldán-Molina, Y. Yuan, K. Lenz, J. Lindner, P. Landeros, and J. Fassbender, *Phys. Rev. B* **99**, 024426 (2019).
- ¹⁶V. E. Demidov, M. P. Kostylev, K. Rott, J. Munchenberger, G. Reiss, and S. O. Demokritov, *Appl. Phys. Lett.* **99**, 082507 (2011).
- ¹⁷P. Klein, R. Varga, and M. Vázquez, *J. Phys. D: Appl. Phys.* **47**, 255001 (2014).
- ¹⁸Z. Duan, I. Krivorotov, R. Arias, N. Reckers, S. Stienen, and J. Lindner, *Phys. Rev. B* **92**, 104424 (2015).
- ¹⁹C. Bayer, J. Jorzick, B. Hillebrands, S. Demokritov, R. Kouba, R. Bozinoski, A. Slavin, K. Guslienko, D. Berkov, N. Gorn, and M. P. Kostylev, *Phys. Rev. B* **72**, 064427 (2005).
- ²⁰V. Demidov, U.-H. Hansen, and S. Demokritov, *Phys. Rev. Lett.* **98**, 157203 (2007).
- ²¹T. Sebastian, K. Schultheiss, B. Obry, B. Hillebrands, and H. Schultheiss, *Front. Phys.* **3**, 35 (2015).
- ²²T. Mewes, J. Kim, D. V. Pelekhov, G. N. Kakazei, P. E. Wigen, S. Batra, and P. C. Hammel, *Phys. Rev. B* **74**, 144424 (2006).
- ²³H. Stoll, M. Noske, M. Weigand, K. Richter, B. Krüger, R. Reeve, M. Hänze, C. Adolff, F.-U. Stein, G. Meier, M. Kläui, and G. Schütz, *Front. Phys.* **3**, 26 (2015).
- ²⁴F. Groß, N. Träger, J. Förster, M. Weigand, G. Schütz, and J. Gräfe, *Appl. Phys. Lett.* **114**, 012406 (2019).
- ²⁵V. Sluka, T. Schneider, R. Gallardo, A. Kákay, M. Weigand, T. Warnatz, R. Mattheis, A. Roldán-Molina, P. Landeros, V. Tiberkevich, A. Slavin, G. Schütz, A. Erbe, A. Deac, J. Lindner, J. Raabe, J. Fassbender, and S. Wintz, *Nat. Nanotechnol.* **14**, 328–333 (2019).
- ²⁶S. Bonetti, R. Kukreja, Z. Chen, D. Spoddig, K. Ollefs, C. Schöppner, R. Meckenstock, A. Ney, J. Pinto, R. Houanche, J. Frisch, J. Stöhr, H. Dürr, and H. Ohldag, *Rev. Sci. Instrum.* **86**, 093703 (2015).
- ²⁷M. Weigand, *Realization of a New Magnetic Scanning X-ray Microscope and Investigation of Landau Structures under Pulsed Field Excitation* (Cuvillier Verlag, 2015), ISBN: 978-3-95404-991-2.
- ²⁸T. Schaffers, R. Meckenstock, D. Spoddig, T. Feggeler, K. Ollefs, C. Schöppner, S. Bonetti, H. Ohldag, M. Farle, and A. Ney, *Rev. Sci. Instrum.* **88**, 093703 (2017).
- ²⁹T. Schaffers, T. Feggeler, S. Pile, R. Meckenstock, M. Buchner, D. Spoddig, V. Ney, M. Farle, H. Wende, S. Wintz, M. Weigand, H. Ohldag, K. Ollefs, and A. Ney, *Nanomaterials* **9**, 940 (2019).
- ³⁰C. Kittel, *Phys. Rev.* **110**(6), 1295 (1958).
- ³¹R. Narkowicz, D. Suter, and R. Stonies, *J. Magn. Reson.* **175**, 275 (2005).
- ³²R. Narkowicz, D. Suter, and I. Niemeyer, *Rev. Sci. Instrum.* **79**, 084702 (2008).
- ³³A. Banholzer, R. Narkowicz, C. Hassel, R. Meckenstock, S. Stienen, O. Posth, D. Suter, M. Farle, and J. Lindner, *Nanotechnology* **22**, 295713 (2011).
- ³⁴C. Schöppner, K. Wagner, S. Stienen, R. Meckenstock, M. Farle, R. Narkowicz, D. Suter, and J. Lindner, *J. Appl. Phys.* **116**, 033913 (2014).
- ³⁵A. Vansteenkiste, J. Leliaert, M. Dvornik, M. Helsen, F. Garcia-Sanchez, and B. V. Waeyenberge, *AIP Adv.* **4**, 107133 (2014).
- ³⁶V. Demidov, S. Demokritov, K. Rott, P. Krzysteczko, and G. Reiss, *Phys. Rev. B* **77**, 064406 (2008).
- ³⁷Z. Zhang, M. Vogel, J. Holanda, J. Ding, M. Jungfleisch, Y. Li, J. Pearson, R. Divan, W. Zhang, A. Hoffmann, Y. Nie, and V. Novosad, *Phys. Rev. B* **100**, 014429 (2019).